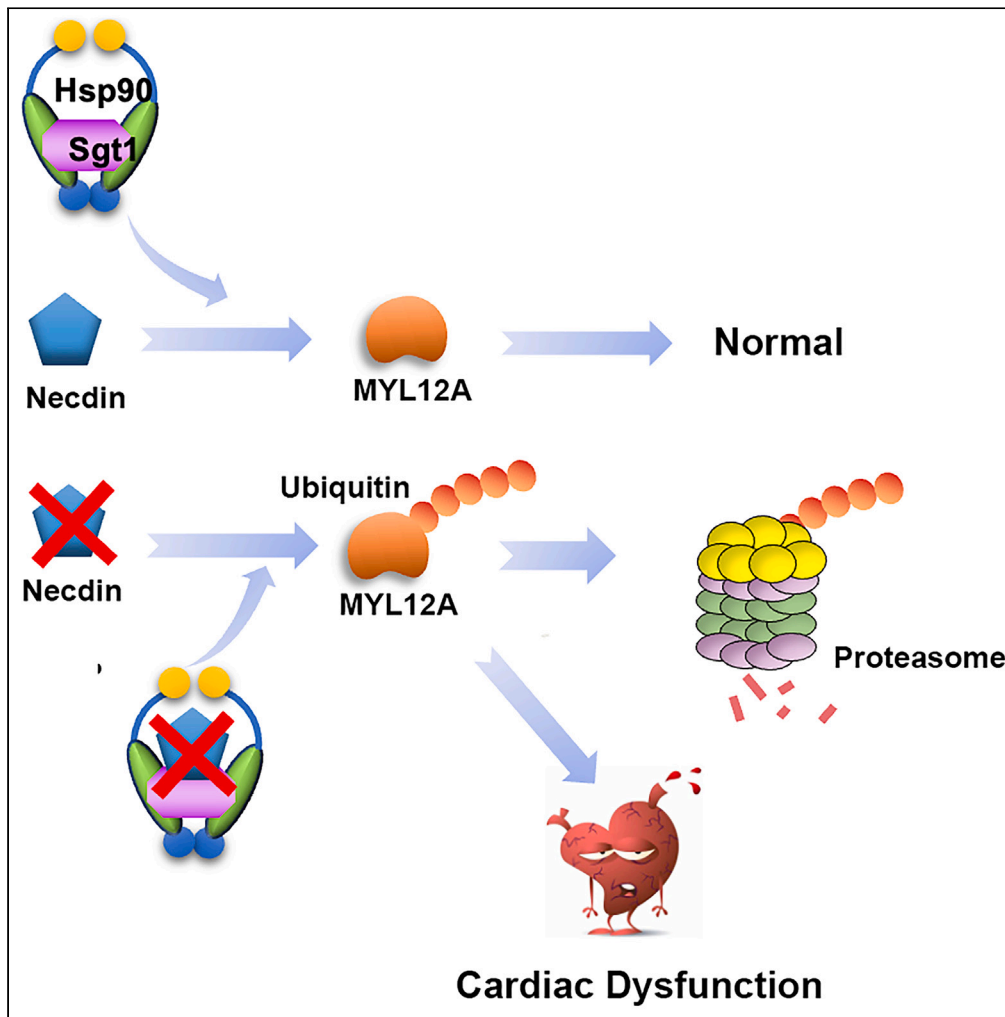


Article

Deficiency in Prader-Willi syndrome gene *necdin* leads to attenuated cardiac contractility



Yufan Dong,
Renbin Lu, Hui
Cao, Jing Zhang,
Xiushan Wu, Yun
Deng, Jia-Da Li

dengyun@hunnu.edu.cn (Y.D.)
lijjada@sklmg.edu.cn (J.-D.L.)

Highlights

Necdin deficiency resulted in heart dysfunction in mice

Necdin stabilized MYL12A through SGT1-HSP90 chaperone machinery

Cardiac-specific overexpression of MYL12A rescued the dysfunction in necdin-deficient mice



Article

Deficiency in Prader-Willi syndrome gene *necdin* leads to attenuated cardiac contractilityYufan Dong,^{1,5,8} Renbin Lu,^{1,5,8} Hui Cao,^{6,7,8} Jing Zhang,^{1,2,3} Xiushan Wu,^{6,7} Yun Deng,^{6,7,*} and Jia-Da Li^{1,2,3,4,5,9,*}

SUMMARY

Prader-Willi syndrome (PWS) is a genetic disorder characterized by behavioral disturbances, hyperphagia, and intellectual disability. Several surveys indicate that PWS is also associated with cardiac abnormalities, possibly contributing to a high incidence of sudden death. However, the pathological mechanisms underlying cardiac dysfunction in PWS remain unclear. In this study, we found that deficiency in *necdin*, an intronless gene within PWS region, led to heart systolic and diastolic dysfunction in mice. Through yeast two-hybrid screening, we identified an interaction between *necdin* and non-muscle myosin regulatory light chain 12a/b (MYL12 A/B). We further showed that *necdin* stabilized MYL12 A/B via SGT1-heat shock protein 90 (HSP90) chaperone machinery. The zebrafish lacking the MYL12 A/B analog, MYL12.1, exhibited impaired heart function, while cardiac-specific overexpression of MYL12A normalized the heart dysfunction in *necdin*-deficient mice. Our findings revealed *necdin* dysfunction as a contributing factor to cardiomyopathy in PWS patients and emphasized the importance of HSP90 chaperone machinery and non-muscle myosin in heart fitness.

INTRODUCTION

Prader-Willi syndrome (PWS) is caused by loss of function in the paternally derived chromosome 15q11-q13,¹ a maternally imprinted region.² This region includes a few protein-coding genes (*MKRN3*, *MAGEL2*, *NDN*, *SNRPN-SNURF*, and *C15orf2*) and several noncoding RNA transcripts.³ PWS is a rare genetic disorder, with occurrence of 1/10,000 to 1/25,000 in the general population. Patients with PWS show severe hypotonia, characteristic facial features, hypogonadism, intellectual disabilities, behavioral disturbances, excessive eating, and gradual development of morbid obesity.⁴ Furthermore, PWS patients also present with structural and functional cardiac abnormalities.⁵

The mortality rate of PWS patients is about three times higher than the general population (~3% per year), and cardiac problems are among the most common causes of sudden death in PWS patients.^{6,7} However, the pathological mechanisms underlying the cardiac abnormalities in PWS patients remain obscure. It has been postulated that endocrine disturbances⁸ and obesity⁹ are the main causes of cardiovascular diseases in PWS. Most PWS patients are diagnosed with growth hormone deficiency (GHD),¹⁰ whereas GHD is reported to be associated with cardiovascular diseases which can be reversed by growth hormone replacement therapy.^{11–13} In addition, as one of the major characteristics of PWS patients, obesity is closely associated with cardiovascular diseases through obesity-induced inflammation, oxidative stress, and altered plasma lipoproteins.¹⁴

However, much evidence has emerged suggesting that the heart defects in PWS patients also show some inherited traits. A retrospective cohort study in 2015 found that heart defects are the most frequent congenital defects in PWS.¹⁵ Marcus et al. performed electrocardiographic recordings and two-dimensional speckle tracking echocardiography to evaluate the cardiac anatomy and myocardial systolic function in children with PWS and found structural and systolic myocardial deformation abnormalities in all three directions (longitudinal, circumferential and radial).¹⁶ Nevertheless, the mechanism of cardiac dysfunction in PWS is still unclear.

NDN, an intronless gene within the PWS region, encodes *necdin*, a protein with 321 amino acid residues.¹⁷ *Neecdin* is involved in a variety of physiological functions, including adipogenesis,¹⁸ myogenesis,^{19,20} as well as neuronal differentiation, survival, and migration.^{21–23} In this study, we found that deletion of *necdin* leads to attenuated cardiac contractility in mice. In order to further study the molecular mechanism, we used a yeast two-hybrid library screening system and found that *necdin* interacted with myosin regulatory light chain 12a (MYL12A), a

¹Center for Medical Genetics, School of Life Sciences, Central South University, Changsha 410078, Hunan, P.R. China

²Hunan Key Laboratory of Animal Models for Human Diseases, Changsha 410078, Hunan, P.R. China

³Hunan Key Laboratory of Medical Genetics, Changsha 410078, Hunan, P.R. China

⁴Hunan International Scientific and Technological Cooperation Base of Animal Models for Human Diseases, Changsha 410078, Hunan, P.R. China

⁵National Clinical Research Center for Geriatric Disorder, Xiangya Hospital, Central South University, Changsha 410078, Hunan, P.R. China

⁶State Key Laboratory of Developmental Biology of Freshwater Fish, Hunan Normal University, Changsha, China

⁷Laboratory of Zebrafish Genetics, College of Life Sciences, Hunan Normal University, Changsha, China

⁸These authors contributed equally

⁹Lead contact

*Correspondence: dengyun@hunnu.edu.cn (Y.D.), lijiaada@sklmg.edu.cn (J.-D.L.)

<https://doi.org/10.1016/j.isci.2024.109974>



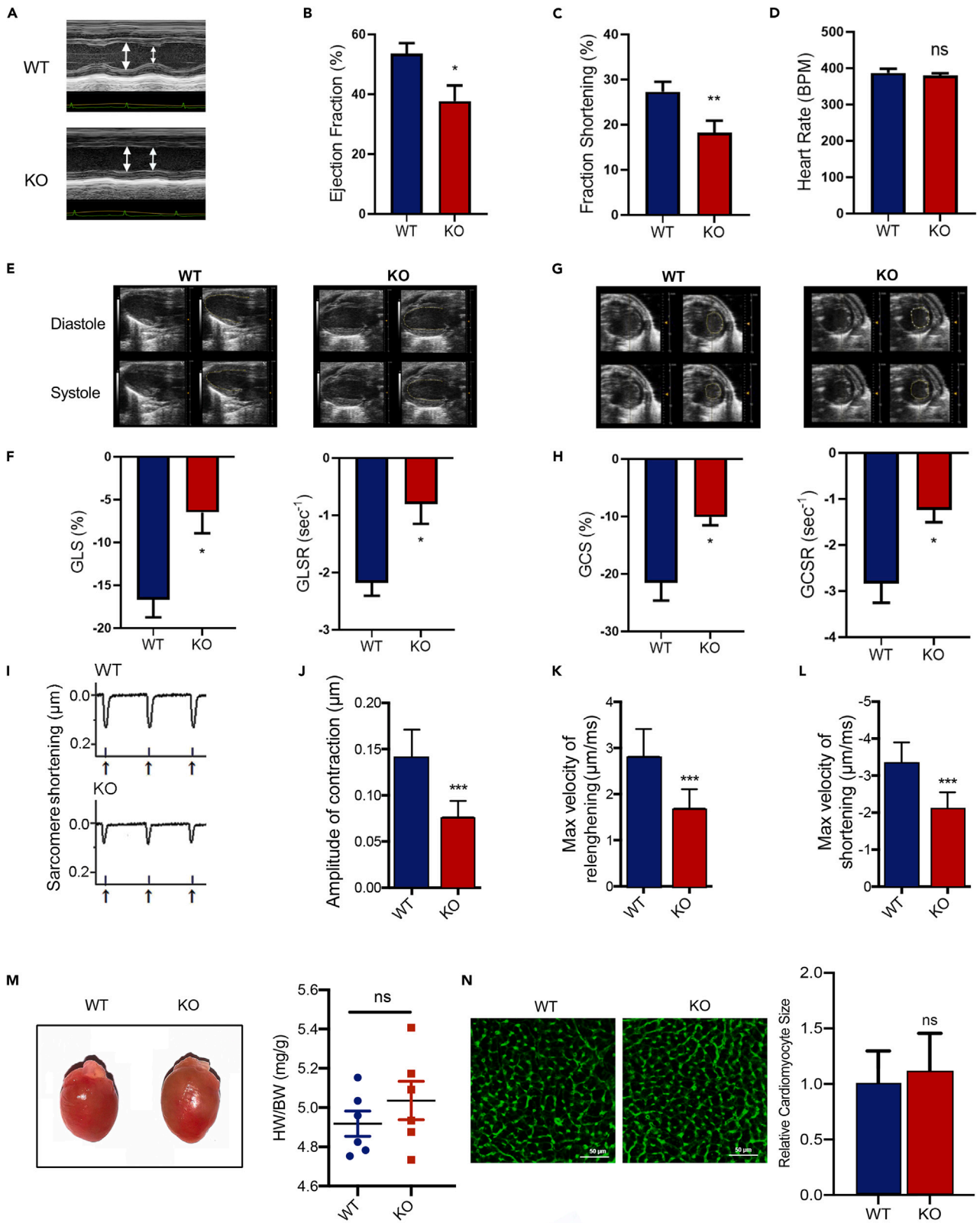


Figure 1. *Necdin* deficiency impaired heart function

(A) Representative M-mode images (upper: wild-type mouse; lower: *necdin* KO mouse). Double-headed arrows mark left ventricle systolic and diastolic internal diameters (LVIDs and LVIDd), respectively.

(B–D) Quantification of echocardiograms: ejection fraction (B), fraction shortening (C), and heart rate (D). Data are presented as means \pm SEM; WT: $n = 14$; KO: $n = 11$; * $p < 0.05$, ** $p < 0.01$, unpaired t test.

(E–H) Echocardiographic image acquisition and speckle-tracking analysis. (E) Representative long-axis B-mode images of left ventricle during diastole and systole period in WT or KO mice. The tracking trace was overlaid on the images showing in the right panels. (F) The global longitudinal strain (GLS) and global longitudinal strain rates (GLSR) in 3 pairs of 4 months male mice. (G) Representative short-axis B-mode images of left ventricle during diastole and systole period in WT or KO mice. The tracking trace was overlaid on the images showing in the right panels. (H) The global circumferential strain (GCS) and GCS rates in 3 pairs of 4 months male mice. Data are presented as means \pm SEM; * $p < 0.05$, unpaired t test.

(I) Representative contraction of cardiac myocytes from WT and KO mice at 4 months of age.

(J–L) Quantification of cardiac myocyte contraction: amplitude of contraction (J), maximal velocity of re-lengthening (K), and maximal velocity of shortening (L). Data are presented as means \pm SEM, WT: $n = 24$; KO: $n = 24$; * $p < 0.05$, ** $p < 0.01$ and *** $p < 0.001$, unpaired t test.

(M) Representative gross anatomy from a WT and a KO mouse at 4 months of age. Statistical data are shown as means \pm SEM, WT: $n = 6$; KO: $n = 6$; ns: no significant difference, unpaired t test.

(N) Cardiomyocyte cross-sectional area (using wheat-germ-agglutinin staining) from WT and KO mice at 4 months. Statistical data are shown as means \pm SEM, WT: $n = 6$; KO: $n = 6$; ns: no significant difference, unpaired t test. Scale bars: 50 μm .

non-muscle myosin regulatory light-chain protein. Additionally, we found that *necdin* interacted with SGT1/heat shock protein 90 (HSP90) chaperone machinery to stabilize MYL12A. Disruption of *necdin* or SGT1 expression destabilized MYL12A by promoting its degradation through the ubiquitin system. Importantly, MYL12.1 deficiency resulted in heart dysfunction in zebrafish, whereas *trans*-cardiac overexpression of MYL12A in *necdin*-deficient mice rescued the cardiac phenotypes.

RESULTS***Necdin* deficiency caused attenuated cardiac contractility in mice**

To determine the cardiac function of *Necdin*, we compared the echocardiography of wild-type (WT) and *necdin*-deficient (knockout [KO]) mice. As shown in Figures 1A–1C and Table S1, the ejection fraction and left ventricular fractional shortening were significantly decreased in KO mice as compared with WT mice. However, there was no difference in heart rate between WT and KO mice (Figure 1D). Furthermore, KO mice also showed significantly lower global longitudinal strain (GLS) and GLS rate (Figures 1E and 1F) as well as global circumferential strain (GCS) and GCS rate (Figures 1G and 1H), as determined by the speckle-tracking analysis.

We also analyzed the other diastolic function parameters, including *in vitro* release test, E/A ratio, and left ventricular (LV) myocardial performance index from *necdin*-KO versus WT mice (Table S2). There is no genotypic difference in these parameters. Further, we measured the contraction of cardiomyocytes isolated from WT and KO mice. Cardiomyocytes from the KO mice showed a significant decrease in contraction amplitude as well as in velocity of shortening and re-lengthening (Figures 1I and 1L), whereas the basal sarcomere lengths were comparable in myocytes from WT and KO mice (Figure S1A). Cytoplasmic calcium concentration is a significant factor activating the ATPase on the myosin head and is a prerequisite for triggering myocardium contraction.^{24,25} Therefore, we also measured intracellular calcium transients of cardiomyocytes from WT and KO mice under constant stimulation. There was no difference in either calcium concentration changes (Figures S1B and S1C) or the velocity of $[\text{Ca}^{2+}]_i$ transients (Figures S1D and S1E) between these two groups. Moreover, the hearts from WT or KO mice were comparable in morphology, heart weight, and ventricle wall thicknesses (Figures 1M and S2A–S2C). Meanwhile, the cross-sectional areas of cardiomyocytes were not significantly changed in KO mice (Figure 1N). Trichrome staining of heart sections also revealed no interstitial fibrosis in KO mice (Figure S3). Taken together, our results suggest that *necdin* deficiency leads to systolic heart dysfunction in mice.

***Necdin* interacted with MYL12A**

To study the underlying mechanism by which *necdin* affects heart function, we performed yeast two-hybrid screening using *necdin* as bait (Table S3). Among the *necdin*-interactive proteins, MYL12A attracted our attention. Firstly, the *Myl12a* gene was identified as a cardiovascular disease risk gene in a genome-wide association study.²⁶ Secondly, MYL12A functions as a key regulatory light chain for non-muscle myosin II B (NMIIB), and an accumulating body of genetic research consistently suggests the potential implication of NMIIB in heart diseases. We confirmed the *Necdin*-MYL12A interaction in a yeast two-hybrid system: only yeast colonies co-transformed with both pGBKT-*necdin* and pGADT7-*Myl12a* plasmids grew and became blue on high-stringency plates (SD/-Trp/-Leu/AbA/X- α -Gal), whereas no colonies grew when yeast was transformed with pGBKT7-*necdin* and pGADT7, or pGBKT7 and pGADT7-*Myl12a* (Figure 2A).

We further verified the interaction between *necdin* and MYL12A by using co-immunoprecipitation (coIP). As shown in Figure 2B, the antibody against FLAG was able to pull down HA-tagged MYL12A only when it was co-expressed with FLAG-tagged *necdin* in H9C2 cells; furthermore, an antibody against HA was able to pull down FLAG-*necdin* only when it was co-expressed with HA-tagged MYL12A. We also performed coIP in H9C2 cells with antibodies against *necdin*, MYL12A, or control IgG. As shown in Figure 2C, MYL12A was detected in the immunocomplex pulled down by *necdin* antibody, but not by control IgG. Likewise, *necdin* could only be detected in the immunocomplex pulled down by MYL12A antibody, but not by control IgG, indicating that *necdin* interacts with MYL12A endogenously.

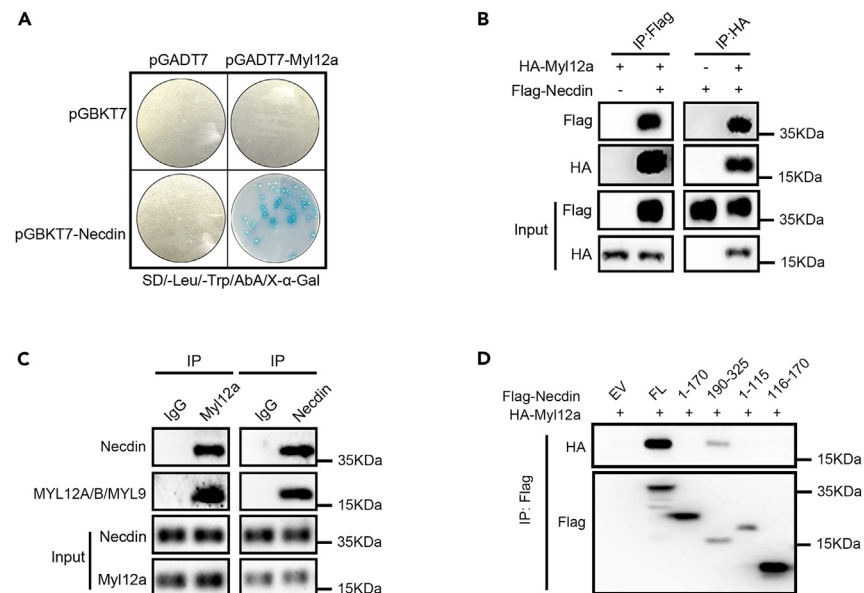


Figure 2. Necdin interacted with MYL12A

(A) Interaction of necdin and MYL12A as assessed with a yeast two-hybrid assay. The term pGBKT7-necdin denotes necdin fused to a DNA-binding domain, whereas pGADT7-My12a denotes My12a fused to an activation domain. Only yeast colonies co-transformed with pGADT7-My12a and pGBKT7-necdin could grow and turn blue on an SD/-Leu/-Trp/AbA/X- α -Gal plate.

(B) Interaction of necdin and MYL12A as assessed with a co-immunoprecipitation (coIP) assay. H9C2 cells were transfected with the indicated plasmids, and protein lysates were precipitated with antibodies against HA or Flag. Immune complexes were blotted with antibody against HA or Flag, respectively.

(C) Necdin interacts with MYL12A endogenously as assayed with a coIP assay in H9C2 cells. Cell lysates were immunoprecipitated with antibodies against necdin, MYL12A, or control IgG, and immune complexes were blotted with antibodies against necdin or MYL12A, respectively.

(D) Interaction of MYL12A and full-length or truncated necdin as assayed by a coIP assay. HA-tagged MYL12A and FLAG-tagged necdin fragments were expressed in H9C2 cells; the cell lysate was immunoprecipitated with Flag antibody, and the immune complex was blotted with HA antibody and Flag antibody, respectively.

To determine which domains in necdin might be involved in the interaction with MYL12A, we performed coIP using full-length necdin or several truncated necdin fragments (amino acids 1–115, 1–170, 116–170, and 190–325). As shown in Figure 2D, only full-length necdin and the 190–325 amino acid fragment interacted with MYL12A.

Necdin stabilized MYL12 A/B/MYL9 protein

To study the functional consequences of the necdin-MYL12A interaction, we compared MYL12A in the heart and other tissues from WT and KO mice. As shown in Figures 3A, 3B, and S4A, MYL12A protein levels were significantly decreased in the KO mouse as compared to WT controls in the heart, spleen, lung, and kidney. Moreover, overexpression of necdin increased the MYL12A protein level, whereas knockdown of *necdin* with siRNAs significantly downregulated the endogenous MYL12A protein level in H9C2 cells (Figures 3C–3F).

As necdin deficiency in mice had no effect on the transcription of MYL12A in the heart (Figure S4B), we speculate that necdin may regulate MYL12A protein stability. Indeed, knockdown of *necdin* significantly decreased the half-life of MYL12A (Figures 3G and 3H). Furthermore, knockdown of *necdin* significantly increased MYL12A ubiquitination (Figure 3I), indicating that depletion of necdin destabilizes MYL12A through the ubiquitin pathway.

As MYL12A has high similarity with MYL12B and MYL9 (Figure S5A), the antibody recognizing MYL2A cannot distinguish between them. MYL12B has lower expression in heart while MYL9 is highly expressed there,²⁷ which prompted us to study whether Necdin can regulate MYL9 protein levels. As expected, overexpression of necdin increased exogenous MYL9 protein level (Figures S5B and S5C). However, there was no genotypic difference in the protein levels of MYL2 and MYL7, two cardiac myosin regulatory light chains (Figures S6A and S6B). Taken together, our results indicate that necdin can regulate MYL12A and MYL9 protein levels, but has no effect on MYL2 or MYL7.

Necdin stabilized MYL12A through SGT1-HSP90 chaperone machinery

As SGT1, a co-chaperone of HSP90, is another necdin-interactive protein identified from the yeast two-hybrid screening, we wondered if the SGT1-HSP90 machinery is involved in the stabilization of MYL12A by necdin. Indeed, MYL12A, necdin, and SGT1 form a complex, as MYL12A and SGT1 were detected in the immunocomplex pulled down by necdin antibody, and MYL12A and necdin were detected in the immunocomplex pulled down by SGT1 antibody (Figure 4A).

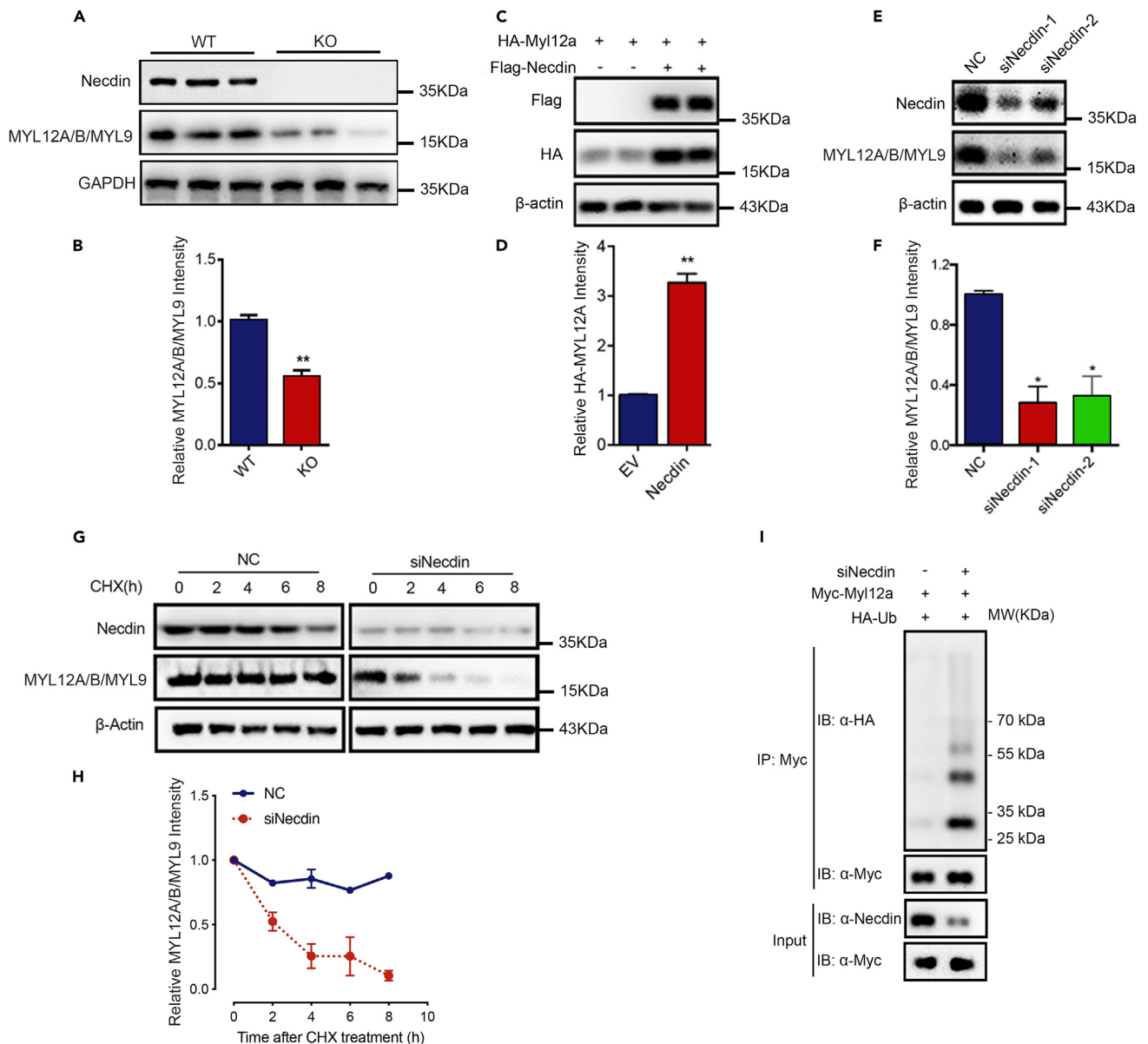


Figure 3. Neccdin regulated the stabilization of MYL12A

(A and B) Expression of MYL12A/B/MYL9 in hearts from WT and *neccdin*-deficient (KO) mice. Data are presented as means \pm SEM, WT: $n = 3$; KO: $n = 3$; * $p < 0.05$, ** $p < 0.01$ and *** $p < 0.001$, unpaired t test.

(C and D) Overexpression of *neccdin* increased the MYL12A protein levels in H9C2 cells. Representative immunoblots (C) and quantification of three independent experiments (D) are shown. Data are presented as means \pm SEM, $n = 3$; ** $p < 0.01$, unpaired t test.

(E and F) RNA interference of *neccdin* decreased MYL12A in H9C2 cells. Representative immunoblots (E) and quantification of three independent experiments (F) are shown. Data are presented as means \pm SEM, $n = 3$; ** $p < 0.01$, unpaired t test.

(G and H) RNA interference of *neccdin* accelerates the degradation of MYL12A protein levels in H9C2 cells. Cycloheximide (CHX, 200 μ g/mL) was used to inhibit protein synthesis. The representative immunoblots (G) and quantification of three independent experiments (H) are shown. Data are presented as means \pm SEM; * $p < 0.05$, ** $p < 0.01$, *** $p < 0.005$, Bonferroni post hoc analysis, two-way ANOVA; NC, negative control.

(I) RNA interference of *neccdin* increases the ubiquitination level of MYL12A. H9C2 cells were transfected with the indicated plasmids or siRNAs. Cell lysates were immunoprecipitated with an antibody against Myc, and ubiquitination was detected with an anti-HA antibody.

To investigate the effect of SGT1 on MYL12A, we knocked down SGT1 expression using siRNA in H9C2 cells and measured the endogenous MYL12A protein level. As shown in Figures 4B and 4C, depletion of SGT1 significantly decreased MYL12A protein levels. Conversely, overexpression of SGT1 significantly increased MYL12A protein level in H9C2 cells (Figures 4D and 4E). Meanwhile, SGT1 overexpression also increased the exogenous expression of MYL9 (Figure S7). Furthermore, knockdown of SGT1 significantly increased the ubiquitination level of

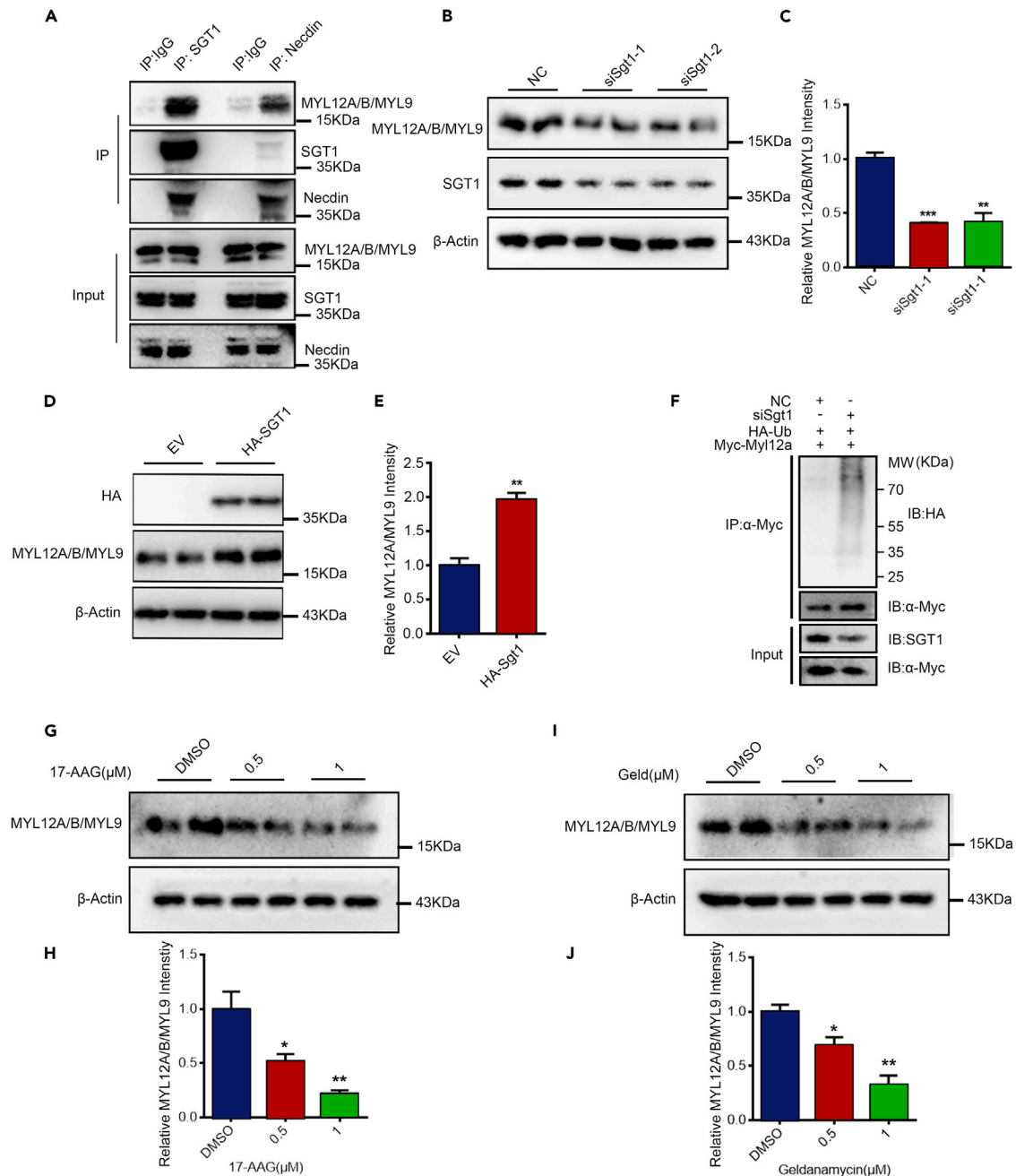


Figure 4. SGT1-HSP90 pathway regulated MYL12A stability

(A) Nectdin-SGT1-MYL12 A/B/MYL9 formed a complex in H9C2 cells. An anti-SGT1 antibody, anti-nectdin antibody, or control IgG was used to immunoprecipitate cell lysate from H9C2 cells; immune-complexes were blotted with the indicated antibodies.

(B and C) RNA interference of Sgt1 decreased MYL12A in H9C2 cells. Representative immunoblots (B) and quantification of three independent experiments each group (C) are shown. Data are presented as means \pm SEM, $n = 3$; ** $p < 0.01$, unpaired t test.

(D and E) Overexpression of SGT1 increased the MYL12A protein levels in H9C2 cells. Representative immunoblots (D) and quantification of three independent experiments (E) are shown. Data are presented as means \pm SEM, $n = 3$; ** $p < 0.01$, unpaired t test.

(F) RNA interference of Sgt1 increases the ubiquitination level of MYL12A. H9C2 cells were transfected with the indicated plasmids or siRNAs. Cell lysates were immunoprecipitated with an antibody against Myc, and ubiquitination was detected with an anti-HA antibody.

(G-J) Representative immunoblots (upper lane) and statistics data of three independent experiments (lower lane) from H9C2 cells following treatment with different concentrations of HSP90 inhibitors 17-AAG (G and H) or geldanamycin (GA) (I and J). Data are presented as means \pm SEM, * $p < 0.05$; ** $p < 0.01$, post hoc Dunnett's t test, one-way ANOVA.

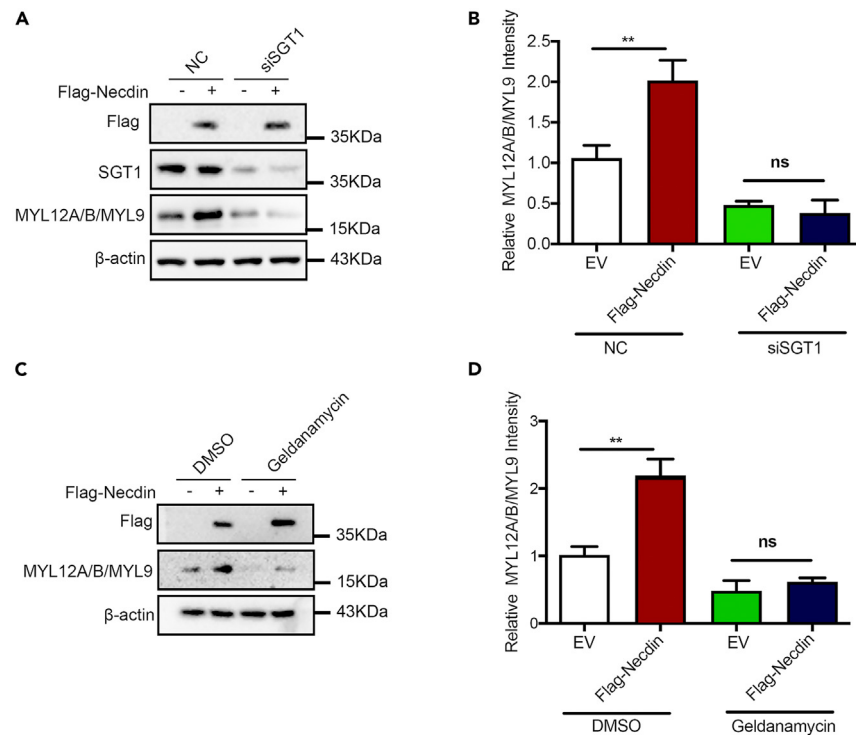


Figure 5. Neccin regulated MYL12A stability in a SGT1- and HSP90-dependent manner

(A and B) Neccin failed to increase MYL12A protein levels in SGT1-depleted (siSGT1) H9C2 cells. Representative immunoblots (A) and statistics data of three independent experiments (B) are shown. Data are presented as means \pm SEM, * p < 0.05, unpaired t test. (C and D) Neccin failed to increase MYL12A protein levels in H9C2 cells treated with HSP90 inhibitor GA. Representative immunoblots (C) and statistics data of three independent experiments (D) are shown. Data are presented as means \pm SEM, * p < 0.05, unpaired t test.

MYL12A (Figure 4F). As SGT1 is a co-chaperone for HSP90, we further investigated the effects of HSP90 inhibitors on MYL12A protein levels. As shown in Figures 4G–4J, HSP90 inhibitors 17-AAG and geldanamycin (GA) significantly downregulated MYL12A protein levels.

Interestingly, overexpression of neccin in SGT1-depleted H9C2 cells failed to increase MYL12A protein levels (Figures 5A and 5B), indicating that SGT1 is required for neccin to stabilize MYL12A protein. Furthermore, overexpression of neccin in GA-treated H9C2 cells failed to increase the MYL12A protein level (Figures 5C and 5D), indicating that HSP90 is required for neccin to stabilize MYL12A protein. These results demonstrate that neccin stabilized MYL12A in a SGT1- and HSP90-dependent manner.

MYL12.1 deficiency in zebrafish led to cardiac dysfunction

To investigate the functional role of MYL12 A/B in the heart, we utilized zebrafish as the model organism. Two homologs of mouse Myl12a/b, MYL12.1 and MYL12.2, were identified in zebrafish with a high level of homology (>90%) (Figure S8A). *In situ* hybridization indicated that MYL12.1, but not MYL12.2, was prominently expressed in the heart (Figure 6A).

We then generated MYL12.1 knockout zebrafish using CRISPR-Cas9 technology, and a founder with 2-bp deletion was selected for further investigation (Figures 6B and S8B). The expression of MYL12.1 was barely detectable in the 48 h postfertilization MYL12.1^{-/-} zebrafish embryos (Figure 6C), confirming the successful knockout of MYL12.1 gene. The MYL12.1^{-/-} embryos showed no discernible phenotype during development, but no MYL12.1^{-/-} fish survived to adulthood (Figure 6D). Therefore, we utilized MYL12.1^{+/-} zebrafish for further analysis. The echocardiography analysis revealed considerable reductions in both ejection fraction and fractional shortening in adult MYL12.1^{+/-} zebrafish compared to WT controls, although there was no genotypic difference in the heart rate (Figures 6E–6G). These data indicate an impaired overall LV function in the hearts of MYL12.1^{+/-} zebrafish, which is in coincidence with the cardiac dysfunction in neccin-deficient mice.

Cardiac-specific overexpression of MYL12A rescued cardiac dysfunction in neccin-deficient mice

To demonstrate whether reduced MYL12A is indeed responsible for the heart dysfunction in *neccin*-deficient mice, we injected AAV9 expressing MYL12A or a control virus (AAV9-EGFP) directly into the left ventricle myocardium and measured echocardiography at day 12 after injection (Figure 7A). The expression of FLAG-tagged MYL12A in the heart was ascertained by immunofluorescence (Figure 7B). Intriguingly, cardiac-specific overexpression of MYL12A normalized both ejection fraction and left ventricular fractional shortening in *neccin*-deficient mice to the levels of WT mice (Figures 7C and 7D and Table S4).

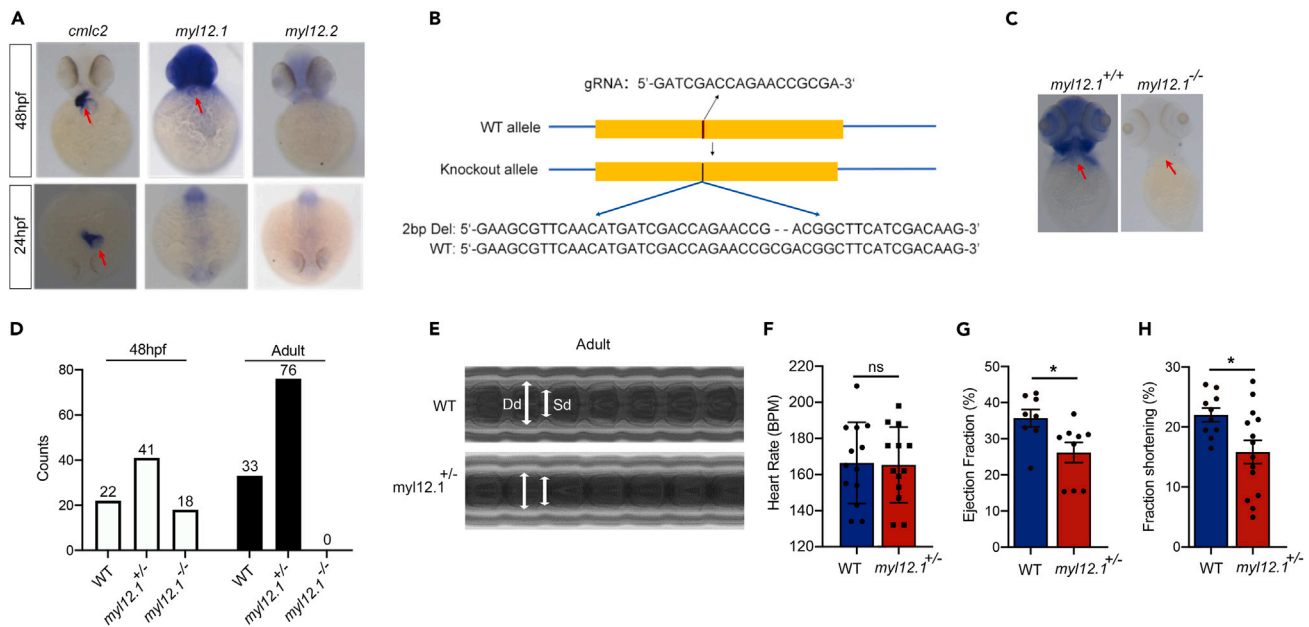


Figure 6. MYL12.1 deficiency in zebrafish led to cardiac dysfunction

(A) The expression of MYL12.1 and MYL12.2 genes in zebrafish heart as analyzed by using whole-mount ISH. Red arrowheads indicate the location of the heart. (B) The CRISPR-Cas9 technique was used to generate MYL12.1 allele in zebrafish. A gRNA targeting the exon 2 of MYL12.1 gene was injected with Cas9 protein into zebrafish embryos, resulting in a 2-bp deletion. (C) ISH was employed to validate the knockout of MYL12.1 in zebrafish. (D) The distribution of different genotypes in the zebrafishes harvested at 48 h postfertilization embryos or in adulthood. (E) Representative M-mode images (upper: wild-type zebrafish; lower: *myl12.1*^{+/-} zebrafish). Double-headed arrows mark ventricle systolic and diastolic internal diameters, respectively. (F–H) The heart rate (F), ejection fraction (G), and fraction shortening (H) of adult WT and MYL12.1^{+/-} zebrafishes as analyzed with echocardiograms. Data are presented as means ± SEM; **p* < 0.05, unpaired t test.

DISCUSSION

In this study, we demonstrated that deficiency of necdin, a protein associated with PWS, led to heart dysfunction, characterized by decreased systolic amplitude and myocardial contraction rate. Mechanistically, necdin interacted with non-muscle MYL12A and stabilized MYL12A through SGT1-HSP90 chaperone machinery. A deficiency in necdin resulted in downregulation of MYL12A, whereas cardiac overexpression of MYL12A rescued the phenotype of attenuated cardiac contractility in *necdin*-deficient mice.

Non-muscle myosin II (NMII) is a hexameric actin-binding protein that is formed of two heavy chains, two essential light chains, and two regulatory light chains (RLCs).²⁸ Conformation and function of NMII are regulated by the phosphorylation of RLCs and the assembly dynamics of myosin filaments. NMII proteins are classified into three subfamilies (i.e., NMIIA, NMIIB, and NMIIIC) according to the heavy-chain isoforms encoded by *Myh9*,²⁹ *Myh10*,³⁰ and *Myh14*,^{31,32} respectively. Mature cardiac myocytes only express NMIIB whereas non-myocytes in the heart express both NMIIA and NMIIB.

Animal studies have suggested that NMIIIs play critical roles in cardiac development. Mice deficient in *Myh10* show severe cardiac dysplasia at an early developmental stage, and mice with a point mutation at a splice donor site in the *Myh10* gene display a phenotype with embryonic hydrocephalus and cardiac defects.³³ Recently, Pandey et al. showed that PKC and non-muscle myosin are upregulated at the costameres in heart diseases, and activation of PKC leads to cardiomyocyte hypertrophy through activation of non-muscle myosin.³⁴

Accumulated genetic studies also suggest the involvement of NMII in heart diseases. For instance, a point mutation in *Myh10* impairs the crosslinkage of NMIIB to actin filaments, interfering with the dynamics of actomyosin cytoskeletal structure, and finally causes defects in heart development and body wall closure.³⁵ There are three highly conserved non-muscle RLCs in mammals: MYL12A, MYL12B, and MYL9 (MYL12A/12B/9).³⁶ Intriguingly, as one of the major non-muscle myosin RLCs, MYL12A has been associated with cardiovascular disease in a genome-wide association study.²⁶ In the present study, we demonstrated that downregulation of the analog of MYL12A, MYL12.1, in zebrafish led to decreased systolic amplitude and myocardial contraction rate, further emphasizing the important role for non-muscle myosins in heart fitness.

Although the NMII and its major RLCs MYL12A have been implicated in heart fitness through genetic studies and animal studies; however, the protein homeostasis processes involved in its regulation remain elusive. We recently demonstrated the interaction between necdin and SGT1, a HSP90 cochaperone protein.³⁷ In this study, we identified MYL12 A/B as another interactive partner of necdin. Therefore,

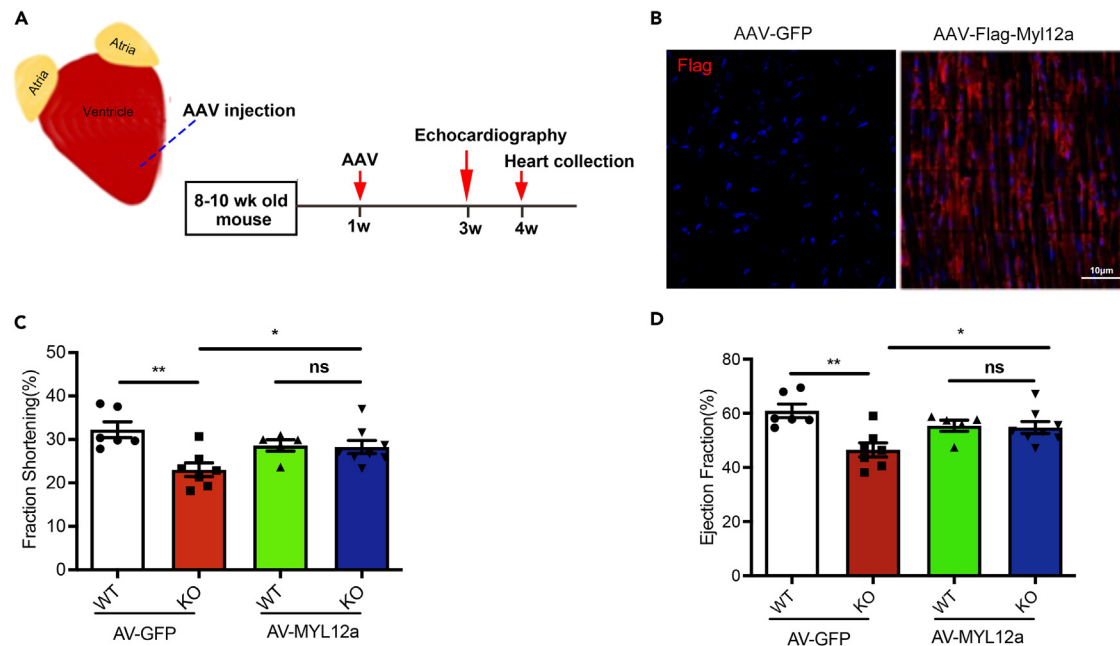


Figure 7. Myocardium delivery of AAV9-Flag-MYL12A in *necdin*-deficient mice rescued cardiomyopathy symptoms

(A) Experimental scheme of virus injection into left ventricle myocardium.

(B) Representative picture of Flag-MYL12A expression after virus injection. Immunofluorescence stained by anti-Flag antibody.

(C-D) Fraction shortening (C) and Ejection fraction (D) quantification of WT and KO mice with or without overexpression of MYL12A. Data are presented as means \pm SEM, * $p < 0.05$; ** $p < 0.01$ unpaired t test.

MYL12A/B-necdin-SGT1-HSP90 may form a complex to stabilize MYL12 A/B protein. Knockout of *necdin* disrupted this complex and destabilized MYL12 A/B, consequently compromising the function of NMII.

HSP90 is a highly conserved and abundant ATP-dependent molecular chaperone. HSP90 functions in a wide variety of cellular processes by facilitating protein remodeling and activation of more than 200 client proteins.³⁸ HSP90 has been generally considered to be cardioprotective, as its inhibitor increases cardiomyocyte apoptosis by downregulation of pro-survival Akt signaling and upregulation of pro-apoptotic p38 α signaling. Cardiac-specific expression of HSP75, the mitochondrial HSP90 homolog, prevented cardiac hypertrophy and fibrosis induced by aortic banding, probably by inhibition of TAK/P38, JNK, and AKT signaling pathways.³⁹ In isolated hearts, HSP90 has also been shown to guide the translocation of PKC ϵ to mitochondria and reduce injury after ischemia/reperfusion insults.⁴⁰ In endothelium, HSP90 plays an integral role in eNOS signaling, a pro-survival mechanism upon activation in cardiomyocytes.⁴¹ Furthermore, the cardioprotective effects of HSP90 may also be mediated by HAX-1 to inhibit IRE-1 signaling at the endoplasmic/sarcoplasmic reticulum level.⁴² In our study, we demonstrated that HSP90 may stabilize non-muscle myosin RLC MYL12A through *necdin* and SGT1. Disruption of *necdin*-SGT1-HSP90 leads to downregulation of MYL12A and reduced contractility of cardiomyocytes.

In summary, our data uncovered an important role for PWS-associated *necdin* in heart fitness, which may underlie the heart dysfunction in PWS patients. It will be intriguing to study the role of *necdin* in the pathophysiology of cardiomyopathy induced by various conditions.

Limitations of the study

Necdin is widely recognized as a key gene associated with PWS. Our study reveals that deficiency in *necdin* leads to reduced systolic amplitude and myocardial contraction rate by destabilizing the MYL12A protein. Although we have elucidated the crucial role of MYL12A through various methods, including generating a zebrafish line with knockout of its analog MYL12.1 and utilizing AAV9 expressing MYL12A virus to rescue the cardiac phenotype of *necdin*-deficient mice, direct evidence of MYL12A's impact on heart function is still lacking. It is necessary to further investigate by generating cardiac MYL12A-deficient mice and conducting echocardiography measurements. Additionally, detailed investigations are required to delineate the signaling cascades or molecular interactions through which MYL12A contributes to myocardial contractions.

STAR★METHODS

Detailed methods are provided in the online version of this paper and include the following:

- KEY RESOURCES TABLE
- RESOURCE AVAILABILITY
 - Lead contact

- Materials availability
- Data and code availability
- **EXPERIMENTAL MODEL AND STUDY PARTICIPANT DETAILS**
- **METHOD DETAILS**
 - Cell culture and transfection
 - Co-immunoprecipitation (Co-IP) assays
 - Ubiquitination assay
 - Western blotting
 - Hematoxylin-eosin (H&E) staining
 - Cardiomyocyte size measurement
 - Cardiac fibrosis measurement
 - Echocardiography
 - Isolation of mouse cardiomyocytes
 - Sarcomere shortening and Ca²⁺ transient measurements in cardiomyocytes
 - *In situ* hybridization in whole-mount zebrafish embryos
 - Generation of the *MYL12.1*^{-/-} zebrafish
 - Characterization of cardiac function in zebrafish
 - Intramyocardial delivery of AAV9 virus
- **QUANTIFICATION AND STATISTICAL ANALYSIS**

SUPPLEMENTAL INFORMATION

Supplemental information can be found online at <https://doi.org/10.1016/j.isci.2024.109974>.

ACKNOWLEDGMENTS

We would like to thank Dr. Edward Sharman for language editing. This project is funded by the National Natural Science Foundation of China (32371218, 81770780, 31972913, 82101960, 31970504), Key Research and Development Programs from Hunan Province (2021DK2001), Guangdong Key Project in "Development of new tools for diagnosis and treatment of Autism" (2018B030335001), Strategic Priority Research Program of Central South University (ZLXD2017004), and China Postdoctoral Science Foundation (No. 2021T140746).

AUTHOR CONTRIBUTIONS

J.-D.L., R.L., and Y. Dong conceived and designed the study. R.L. and Y. Dong performed *in vitro* cell culture, cell biology, and molecular biology experiments. H.C. performed studies in zebrafish model; J.Z. performed echocardiography in mice; J.-D.L., R.L., and Y. Dong wrote the manuscript; and X.W., Y. Deng, and J.-D.L. reviewed and edited the manuscript.

DECLARATION OF INTERESTS

The authors declare no competing interests.

Received: September 25, 2023

Revised: January 2, 2024

Accepted: May 10, 2024

Published: May 14, 2024

REFERENCES

1. Cassidy, S.B., and Driscoll, D.J. (2009). Prader-Willi syndrome. *Eur. J. Hum. Genet.* *17*, 3–13. <https://doi.org/10.1038/ejhg.2008.165>.
2. Angulo, M.A., Butler, M.G., and Cataletto, M.E. (2015). Prader-Willi syndrome: a review of clinical, genetic, and endocrine findings. *J. Endocrinol. Invest.* *38*, 1249–1263. <https://doi.org/10.1007/s40618-015-0312-9>.
3. Kalsner, L., and Chamberlain, S.J. (2015). Prader-Willi, Angelman, and 15q11-q13 Duplication Syndromes. *Pediatr. Clin. North Am.* *62*, 587–606. <https://doi.org/10.1016/j.pcl.2015.03.004>.
4. Cassidy, S.B., Schwartz, S., Miller, J.L., and Driscoll, D.J. (2012). Prader-Willi syndrome. *Genetics in medicine*. *Genet. Med.* *14*, 10–26. <https://doi.org/10.1038/gim.0b013e31822bead0>.
5. Patel, S., Harmer, J.A., Loughnan, G., Skilton, M.R., Steinbeck, K., and Celermajer, D.S. (2007). Characteristics of cardiac and vascular structure and function in Prader-Willi syndrome. *Clin. Endocrinol.* *66*, 771–777. <https://doi.org/10.1111/j.1365-2265.2007.02808.x>.
6. Butler, M.G., Manzardo, A.M., Heinemann, J., Loker, C., and Loker, J. (2017). Causes of death in Prader-Willi syndrome: Prader-Willi Syndrome Association (USA) 40-year mortality survey. *Genet. Med.* *19*, 635–642. <https://doi.org/10.1038/gim.2016.178>.
7. Manzardo, A.M., Loker, J., Heinemann, J., Loker, C., and Butler, M.G. (2018). Survival trends from the Prader-Willi Syndrome Association (USA) 40-year mortality survey. *Genet. Med.* *20*, 24–30. <https://doi.org/10.1038/gim.2017.92>.
8. Marzullo, P., Marcassa, C., Campini, R., Eleuteri, E., Minocci, A., Sartorio, A., Vettor, R., Liuzzi, A., and Grugni, G. (2007). Conditional cardiovascular response to growth hormone therapy in adult patients with Prader-Willi syndrome. *J. Clin. Endocrinol. Metab.* *92*, 1364–1371. <https://doi.org/10.1210/jc.2006-0600>.
9. Butler, M.G., Bittel, D.C., Kibiriyeva, N., and Garg, U. (2006). C-reactive protein levels in

- subjects with Prader-Willi syndrome and obesity. *Genetics in medicine*. *Genet. Med.* 8, 243–248. <https://doi.org/10.1097/01.gim.0000204469.30913.67>.
- Burman, P., Ritzén, E.M., and Lindgren, A.C. (2001). Endocrine dysfunction in Prader-Willi syndrome: a review with special reference to GH. *Endocr. Rev.* 22, 787–799. <https://doi.org/10.1210/edrv.22.6.0447>.
 - Rosen, T., and Bengtsson, B.A. (1990). Premature mortality due to cardiovascular disease in hypopituitarism. *Lancet* 336, 285–288. [https://doi.org/10.1016/0140-6736\(90\)91812-o](https://doi.org/10.1016/0140-6736(90)91812-o).
 - de Boer, H., Blok, G.J., and Van der Veen, E.A. (1995). Clinical aspects of growth hormone deficiency in adults. *Endocr. Rev.* 16, 63–86. <https://doi.org/10.1210/edrv-16-1-63>.
 - Colao, A., Marzullo, P., Di Somma, C., and Lombardi, G. (2001). Growth hormone and the heart. *Clin. Endocrinol.* 54, 137–154. <https://doi.org/10.1046/j.1365-2265.2001.01218.x>.
 - Greenswag, L.R. (1987). Adults with Prader-Willi syndrome: a survey of 232 cases. *Dev. Med. Child Neurol.* 29, 145–152. <https://doi.org/10.1111/j.1469-8749.1987.tb02129.x>.
 - Torrado, M., Foncuberta, M.E., Perez, M.F.d.C., Gravina, L.P., Araoz, H.V., Baialardo, E., and Chertkoff, L.P. (2013). Change in prevalence of congenital defects in children with Prader-Willi syndrome. *Pediatrics* 131, e544–e549. <https://doi.org/10.1542/peds.2012-1103>.
 - Marcus, K.A., van Alfen-van der Velden, J.A.A.E.M., Otten, B.J., Weijers, G., Yntema, H.G., de Korte, C.L., and Kapusta, L. (2012). Cardiac evaluation in children with Prader-Willi syndrome. *Acta Paediatr.* 101, e225–e231. <https://doi.org/10.1111/j.1651-2227.2011.02570.x>.
 - Nakada, Y., Taniura, H., Uetsuki, T., Inazawa, J., and Yoshikawa, K. (1998). The human chromosomal gene for necdin, a neuronal growth suppressor, in the Prader-Willi syndrome deletion region. *Gene* 213, 65–72. [https://doi.org/10.1016/s0378-1119\(98\)00206-6](https://doi.org/10.1016/s0378-1119(98)00206-6).
 - Wijesuriya, T.M., De Ceuninck, L., Masschaele, D., Sanderson, M.R., Carias, K.V., Tavernier, J., and Wevrck, R. (2017). The Prader-Willi syndrome proteins MAGEL2 and necdin regulate leptin receptor cell surface abundance through ubiquitination pathways. *Hum. Mol. Genet.* 26, 4215–4230. <https://doi.org/10.1093/hmg/ddx311>.
 - Deponti, D., François, S., Baesso, S., Sciorati, C., Innocenzi, A., Broccoli, V., Muscatelli, F., Meneveri, R., Clementi, E., Cossu, G., and Brunelli, S. (2007). Necdin mediates skeletal muscle regeneration by promoting myoblast survival and differentiation. *J. Cell Biol.* 179, 305–319. <https://doi.org/10.1083/jcb.200701027>.
 - Bush, J.R., and Wevrck, R. (2010). Loss of Necdin impairs myosin activation and delays cell polarization. *Genesis* 48, 540–553. <https://doi.org/10.1002/dvg.20658>.
 - Yoshikawa, K. (2000). [Molecular mechanisms of differentiation and death of human neurons: with special reference to necdin and APP]. *Nihon Shinkei Seishin Yakurigaku Zasshi* 20, 155–159.
 - Ohman Forslund, K., and Nordqvist, K. (2001). The melanoma antigen genes—any clues to their functions in normal tissues? *Exp. Cell Res.* 265, 185–194. <https://doi.org/10.1006/excr.2001.5173>.
 - Kuwajima, T., Hasegawa, K., and Yoshikawa, K. (2010). Necdin promotes tangential migration of neocortical interneurons from basal forebrain. *J. Neurosci.* 30, 3709–3714. <https://doi.org/10.1523/JNEUROSCI.5797-09.2010>.
 - Kuo, I.Y., and Ehrlich, B.E. (2015). Signaling in muscle contraction. *Cold Spring Harb. Perspect. Biol.* 7, a006023. <https://doi.org/10.1101/cshperspect.a006023>.
 - Orchard, C.H., Eisner, D.A., and Allen, D.G. (1983). Oscillations of intracellular Ca²⁺ in mammalian cardiac muscle. *Nature* 304, 735–738. <https://doi.org/10.1038/304735a0>.
 - Evans, D.S., Avery, C.L., Nalls, M.A., Li, G., Barnard, J., Smith, E.N., Tanaka, T., Butler, A.M., Buxbaum, S.G., Alonso, A., et al. (2016). Fine-mapping, novel loci identification, and SNP association transferability in a genome-wide association study of QRS duration in African Americans. *Hum. Mol. Genet.* 25, 4350–4368. <https://doi.org/10.1093/hmg/ddw284>.
 - Uhlen, M., Fagerberg, L., Hallstrom, B.M., Lindskog, C., Oksvold, P., Mardinoglu, A., Sivertsson, A., Kampf, C., Sjostedt, E., Asplund, A., et al. (2015). Proteomics. Tissue-based map of the human proteome. *Science* 347, 1260419. <https://doi.org/10.1126/science.1260419>.
 - Vicente-Manzanares, M., Ma, X., Adelstein, R.S., and Horwitz, A.R. (2009). Non-muscle myosin II takes centre stage in cell adhesion and migration. *Nat. Rev. Mol. Cell Biol.* 10, 778–790. <https://doi.org/10.1038/nrm2786>.
 - Simons, M., Wang, M., McBride, O.W., Kawamoto, S., Yamakawa, K., Gdula, D., Adelstein, R.S., and Weir, L. (1991). Human nonmuscle myosin heavy chains are encoded by two genes located on different chromosomes. *Circ. Res.* 69, 530–539. <https://doi.org/10.1161/01.res.69.2.530>.
 - Toothaker, L.E., Gonzalez, D.A., Tung, N., Lemons, R.S., Le Beau, M.M., Arnaout, M.A., Clayton, L.K., and Tenen, D.G. (1991). Cellular myosin heavy chain in human leukocytes: isolation of 5' cDNA clones, characterization of the protein, chromosomal localization, and upregulation during myeloid differentiation. *Blood* 78, 1826–1833.
 - Leal, A., Endeles, S., Stengel, C., Huehne, K., Loetterle, J., Barrantes, R., Winterpacht, A., and Rautenstrauss, B. (2003). A novel myosin heavy chain gene in human chromosome 19q13.3. *Gene* 312, 165–171. [https://doi.org/10.1016/s0378-1119\(03\)00613-9](https://doi.org/10.1016/s0378-1119(03)00613-9).
 - Golomb, E., Ma, X., Jana, S.S., Preston, Y.A., Kawamoto, S., Shoham, N.G., Goldin, E., Conti, M.A., Sellers, J.R., and Adelstein, R.S. (2004). Identification and characterization of nonmuscle myosin II-C, a new member of the myosin II family. *J. Biol. Chem.* 279, 2800–2808. <https://doi.org/10.1074/jbc.M309981200>.
 - Ridge, L.A., Mitchell, K., Al-Anbaki, A., Shaikh Qureshi, W.M., Stephen, L.A., Tenin, G., Lu, Y., Lupu, I.E., Clowes, C., Robertson, A., et al. (2017). Non-muscle myosin IIB (Myh10) is required for epicardial function and coronary vessel formation during mammalian development. *PLoS Genet.* 13, e1007068. <https://doi.org/10.1371/journal.pgen.1007068>.
 - Pandey, P., Hawkes, W., Hu, J., Megone, W.V., Gautrot, J., Anilkumar, N., Zhang, M., Hirvonen, L., Cox, S., Ehler, E., et al. (2018). Cardiomyocytes Sense Matrix Rigidity through a Combination of Muscle and Non-muscle Myosin Contractions. *Dev. Cell* 44, 326–336.e3. <https://doi.org/10.1016/j.devcel.2017.12.024>.
 - Ma, X., and Adelstein, R.S. (2014). A point mutation in Myh10 causes major defects in heart development and body wall closure. *Circ. Cardiovasc. Genet.* 7, 257–265. <https://doi.org/10.1161/CIRCGENETICS.113.000455>.
 - Park, I., Han, C., Jin, S., Lee, B., Choi, H., Kwon, Y., Kim, D., Kim, J., Lifirsu, E., Park, W.J., et al. (2011). Myosin regulatory light chains are required to maintain the stability of myosin II and cellular integrity. *Biochem. J.* 434, 171–180. <https://doi.org/10.1042/BJ20101473>.
 - Lu, R., Dong, Y., and Li, J.D. (2020). Necdin regulates BMAL1 stability and circadian clock through SGT1-HSP90 chaperone machinery. *Nucleic Acids Res.* 48, 7944–7957. <https://doi.org/10.1093/nar/gkaa601>.
 - Schopf, F.H., Biebl, M.M., and Buchner, J. (2017). The HSP90 chaperone machinery. *Nat. Rev. Mol. Cell Biol.* 18, 345–360. <https://doi.org/10.1038/nrm.2017.20>.
 - Zhang, Y., Jiang, D.S., Yan, L., Cheng, K.J., Bian, Z.Y., and Lin, G.S. (2011). HSP75 protects against cardiac hypertrophy and fibrosis. *J. Cell. Biochem.* 112, 1787–1794. <https://doi.org/10.1002/jcb.23091>.
 - Budas, G.R., Churchill, E.N., Disatnik, M.H., Sun, L., and Mochly-Rosen, D. (2010). Mitochondrial import of PKCepsilon is mediated by HSP90: a role in cardioprotection from ischaemia and reperfusion injury. *Cardiovasc. Res.* 88, 83–92. <https://doi.org/10.1093/cvr/cvq154>.
 - Chen, J.X., and Meyrick, B. (2004). Hypoxia increases Hsp90 binding to eNOS via PI3K-Akt in porcine coronary artery endothelium. *Lab. Invest.* 84, 182–190. <https://doi.org/10.1038/abinvest.3700027>.
 - Lam, C.K., Zhao, W., Cai, W., Vafiadaki, E., Florea, S.M., Ren, X., Liu, Y., Robbins, N., Zhang, Z., Zhou, X., et al. (2013). Novel role of HAX-1 in ischemic injury protection involvement of heat shock protein 90. *Circ. Res.* 112, 79–89. <https://doi.org/10.1161/CIRCRESAHA.112.279935>.
 - Collier, P., Phelan, D., and Klein, A. (2017). A Test in Context: Myocardial Strain Measured by Speckle-Tracking Echocardiography. *J. Am. Coll. Cardiol.* 69, 1043–1056. <https://doi.org/10.1016/j.jacc.2016.12.012>.
 - Beyhoff, N., Brix, S., Betz, I.R., Klopffleisch, R., Foryst-Ludwig, A., Krannich, A., Stawowy, P., Knebel, F., Grune, J., and Kintscher, U. (2017). Application of Speckle-Tracking Echocardiography in an Experimental Model of Isolated Subendocardial Damage. *J. Am. Soc. Echocardiogr.* 30, 1239–1250.e2. <https://doi.org/10.1016/j.echo.2017.08.006>.
 - Bradford, Y.M., Van Slyke, C.E., Ruzicka, L., Singer, A., Eagle, A., Fashena, D., Howe, D.G., Frazer, K., Martin, R., Paddock, H., et al. (2022). Zebrafish information network, the knowledgebase for Danio rerio research. *Genetics* 220, iyac016. <https://doi.org/10.1093/genetics/iyac016>.
 - Li, M., Zhao, L., Page-McCaw, P.S., and Chen, W. (2016). Zebrafish Genome Engineering Using the CRISPR-Cas9 System. *Trends Genet.* 32, 815–827. <https://doi.org/10.1016/j.tig.2016.10.005>.

STAR★METHODS

KEY RESOURCES TABLE

REAGENT or RESOURCE	SOURCE	IDENTIFIER
Antibodies		
Anti-HA antibody	Abcam	Cat# ab91110; RRID:AB_307019
Anti-Flag antibody	Sigma-Aldrich	Cat# F9291; RRID:AB_439698
Anti-Necdin antibody	Abcam	Cat# ab227908; RRID:AB_2235830
Anti-Myl12a antibody	Santa Cruz Biotechnology	Cat# sc-9449; RRID:AB_2250740
Anti-β-actin antibody	Abcam	Cat# ab8226; RRID:AB_306371
Anti-Myc antibody	Cell Signaling Technology	Cat# 2276 (also 2276S); RRID:AB_331783
Anti-SGT1 antibody	Abcam	Cat# ab99293; RRID:AB_10675547
Chemicals, peptides, and recombinant proteins		
CHX	AbMole	M4879
MG-132	MCE	HY-13259
Geldanamycin	MCE	HY-15230
17-AAG	MCE	HY-10211
Critical commercial assays		
RevertAid First Strand cDNA Synthesis Kit	Thermo Scientific	K1622
SYBR™ Green PCR Master Mix	Thermo Scientific	4309155
Trichrome Stain Kit (Connective Tissue Stain)	Abcam	ab150686
Matchmaker® Gold Yeast Two-Hybrid System	Takara	630489
Experimental models: Cell lines		
293FT cells	Thermo Scientific	Cat# R70007
H9c2	ATCC	Cat# CRL-1446
Experimental models: Organisms/strains		
Necdin knockout mouse	Lu et al.2020 ³⁷	N/A
Oligonucleotides		
siRNA targeting sequence for Necdin #1: CCUGCACACCAUGGAGUUUTT	This paper	N/A
siRNA targeting sequence for Necdin #2: UCAUGAUCCUGAGCCUCAUTT	This paper	N/A
siRNA targeting sequence for Sgt1 #1: GCAGAUGUAAAGAACCUAUTT	This paper	N/A
siRNA targeting sequence for Sgt1 #2: CUGGUAUCAACAGAAUCUTT	This paper	N/A
Recombinant DNA		
pcDNA3.1(–)	Invitrogen	Cat# V795-20
pcDNA3.1-HA-Myl12a	This paper	N/A
pcDNA3.1-Flag-Necdin	This paper	N/A
pcDNA3.1-Flag-Necdin (1-170aa)	This paper	N/A
pcDNA3.1-Flag-Necdin (190-325aa)	This paper	N/A
pcDNA3.1-Flag-Necdin (1-115aa)	This paper	N/A
pcDNA3.1-Flag-Necdin (116-170aa)	This paper	N/A
pcDNA3.1-HA-Ubiquitin	This paper	N/A

(Continued on next page)

Continued

REAGENT or RESOURCE	SOURCE	IDENTIFIER
Software and algorithms		
ImageJ	NIH	https://imagej.nih.gov/ij/
Prism	GraphPad	https://www.graphpad.com/scientific-software/prism/

RESOURCE AVAILABILITY**Lead contact**

Requests for resources and reagents should be directed to the lead contact Jia-Da Li (lijidaa@sklimg.edu.cn).

Materials availability

All unique/stable reagents generated in this study are available from the [lead contact](#) with a completed Materials Transfer Agreement.

Data and code availability

Data reported in this paper will be shared by the [lead contact](#) upon request. This paper does not report original code. Any additional information required to reanalyze the data reported in this paper is available from the [lead contact](#) upon request.

EXPERIMENTAL MODEL AND STUDY PARTICIPANT DETAILS

Mice of the same sex were group-housed (3–5 animals per cage) under controlled conditions (temperature, $20 \pm 2^\circ\text{C}$; relative humidity, 50–60%; 12:12-h light-dark (LD) cycle, lights on at 7:00 a.m. and lights off at 7:00 p.m.) and had free access to food and water. 4-month-old wild-type and Necdin knockout male mice were utilized for echocardiographic assessments. In the rescue assay, intramyocardial delivery of AAV9 virus was conducted in 3-month-old wild-type and Necdin knockout male mice, with subsequent echocardiographic measurements taken at day 12 post-injection. All procedures regarding the care and use of animals were approved by the Institutional Animal Care and Use Committee of Central South University of China.

METHOD DETAILS**Cell culture and transfection**

H9C2 rat cardiomyoblast cells (ATCC, USA) were maintained in Dulbecco's modified Eagle's medium (DMEM) supplemented with 10% fetal bovine serum (FBS), 100 units/ml penicillin, and 100 $\mu\text{g}/\text{mL}$ streptomycin at 37°C in 5% CO_2 incubators. Plasmids and siRNA were transfected into cells using Lipofectamine 2000 (Invitrogen) according to the manufacturer's protocol.

Co-immunoprecipitation (Co-IP) assays

Cells were lysed with co-IP buffer (20 mM Tris-HCl, 150 mM NaCl, 1 mM EDTA, 1% Triton X-100, and protease inhibitor cocktail, pH 7.4). After centrifugation, the supernatant was incubated with 30 μL protein G agarose bead slurry (Sigma; P3296) and 1 μg of the indicated antibody or control IgG with constant agitation overnight at 4°C . Beads were collected by centrifugation, pellets were washed extensively 3–5 times with lysis buffer, and boiled with SDS loading buffer for 5 min. The immune complex was detected by Western blot with the indicated antibodies.

Ubiquitination assay

H9C2 cells were transfected with plasmids expressing Myc-MYL12A and HA-ubiquitin, together with control siRNAs, necdin or Sgt1 siRNAs. At 36 h after transfection, cells were treated with MG132 (10 μM) for 9 h to inhibit protein degradation. Cells were then lysed with ubiquitination buffer I (2% SDS, 10 mM Tris-base, pH 7.5, 150 mM NaCl) at 100°C for 10 min. The lysates were then diluted 10-fold with ubiquitination buffer II (1% Triton-100, 10 mM Tris-base, pH 7.5, 2 mM EDTA, 150 mM NaCl) and subjected to immunoprecipitation by using a Myc antibody. The immune complex was detected by Western blot with antibodies against HA and Myc.

Western blotting

Samples were boiled in SDS lysis buffer (2% SDS, 63 mM Tris-HCl, and 10% glycerol) for 5 min. Proteins were separated by SDS-PAGE, and transferred to nitrocellulose membranes. After blocking with blocking buffer (5% skimmed milk in 1% TBST), the membranes were incubated with the indicated primary antibodies overnight at 4°C . After extensive washing, membranes were incubated with horseradish peroxidase conjugated secondary antibodies. The proteins were visualized using the Pierce ECL Western Blotting Substrate kit (Thermo Scientific; 32106). Band intensities were quantified using ImageJ.

Hematoxylin-eosin (H&E) staining

For histological analysis, 20 μm sections from hearts were dried at 65°C for 2 h, and subjected to H&E staining. The sections were stained with hematoxylin for 1 min, and then destained with 1% hydrochloric acid in alcohol for about 30 s. After rinsing with tap water, the sections were stained with eosin carbonate for 30 s. After dehydration, the sections were cleared in xylene for 15 min.

Cardiomyocyte size measurement

To quantify cardiomyocyte size, paraffin-embedded heart sections were stained with FITC–wheat germ agglutinin (Sigma, L4895, 10 $\mu\text{g}/\text{mL}$) for 30 min at room temperature to visualize cell membranes. Images were captured with a fluorescence microscope (Leica TCS SP5) and analyzed by ImageJ software.

Cardiac fibrosis measurement

Hearts were perfused and excised from sodium pentobarbital-euthanized mice, and washed in cold phosphate buffered saline (PBS). The hearts were then fixed in 4% paraformaldehyde, embedded in Tissue-Tek OCT media, and sectioned at 20 μm thickness. Collagen was quantified by Masson's trichrome staining according to the manufacturer's protocol (Abcam; ab150686).

Echocardiography

Echocardiographic measurements were performed under anesthesia (3% isoflurane induction, 1% maintenance) using a VisualSonics Vevo 2100 Imaging System with an MS400 linear array transducer (VisualSonics, Toronto, Canada). Respiration rate (RR) and heart rate (HR) were monitored and kept consistent (100 times/min and 400 beats/min respectively). Images of the cross-sectional view of the left ventricle (LV) at the papillary muscle-level in parasternal short-axis (PSAX) view were obtained and analyzed by using VevoLab software. All image analyses were performed by a single observer using Vevo LAB (FUJIFILM VisualSonics). The following parameters were measured over three cardiac cycles: thickness of the interventricular septum (IVS), LV interior diameter (LVID), and LV posterior wall (LVPW) and used to make the following calculations (via the VevoLab software): ejection fraction (EF; $100 \times ((\text{LV Vol}; \text{d-LV Vol}; \text{s})/\text{LV Vol}; \text{d})$), fractional shortening (FS; $100 \times ((\text{LVID}; \text{d-LVID}; \text{s})/\text{LVID}; \text{d})$), stroke volume (SV; $\text{LV Vol}; \text{d-LV Vol}; \text{s}$), LV mass ($1.053 \times (\text{LVID}; \text{d+LVPW}; \text{d+IVS}; \text{d})^3 - \text{LVID}; \text{d}^3$), and cardiac output (CO; $\text{SV} \times \text{HR}$). From B-mode images, we performed speckle-tracking analysis along the long-axis and short-axis of LV. We followed previous study for speckle tracking analysis.^{43,44} Briefly, using speckle-tracking based strain analysis of 2D B-mode images acquired from the parasternal long- and short-axis views, strain and SR were quantified in the longitudinal and circumferential axes. Global longitudinal strain (GLS) was calculated as $(\text{Ls} - \text{Ld})/\text{Ld}$, where Ls is the longitudinal strain during systole period, and Ld is that in diastole period, based on Lagrangian and Eulerian strain tensors of finite deformation theory. Similarly, global circumferential strain (GCS) was calculated as $(\text{Cs} - \text{Cd})/\text{Cd}$. Global longitudinal strain rate (GLSR) and global circumferential strain rate (GCSR) were the GLS or GCS per second respectively.

Isolation of mouse cardiomyocytes

Mice (16-week of age) were weighed and anesthetized with sodium pentobarbital (50 mg/kg), after injection with 200 μL heparin (100 IU/mouse), for 15 min. Hearts were excised and transferred to a 100-mm dish containing Ca^{2+} -free Tyrode's solution (140 mM NaCl, 5.4 mM KCl, 1.2 mM MgCl_2 , 0.33 mM NaH_2PO_4 , 10 mM glucose and 10 mM HEPES). Each heart was cannulated rapidly followed by treating with Ca^{2+} -free Tyrode solution for 5 min until the effluent became clear. The heart was then treated with enzyme-containing Krebs-Ringer (KRS) solution and HEPES (10 mM) for 20 min; digestion was stopped by addition of KB solution (70 mM KOH, 20 mM taurine, 50 mM glutamic acid, 40 mM KCl, 20 mM NaH_2PO_4 , 3 mM MgSO_4 , 0.5 mM EGTA, 10 mM glucose, 10 mM HEPES) for 5 min. Left ventricular tissues were removed from the heart, transferred to a 100-mm dish and gently agitated with a wide tipped pipette until the single myocytes were gently dispersed; then cells were filtered with a nylon mesh filter and stored at 4°C in KB solution containing 1% BSA until use.

Sarcomere shortening and Ca^{2+} transient measurements in cardiomyocytes

Cardiomyocytes chosen for cell shortening and Ca^{2+} transient measurements have $>1.70 \mu\text{m}$ resting sarcomere length and do not have spontaneous contractions. Cell shortening and Ca^{2+} transients were recorded simultaneously by combinational use of a television monitor (Model IX-70, Olympus, Japan) connected to a video edge detector and a dual-excitation fluorescence photomultiplier system (IonOptix, Milton, MA, USA). For cell shortening studies, freshly isolated cardiomyocytes were continuously superfused at 1 mL/min with Krebs-Henseleit buffer containing 2 mmol/L Ca^{2+} and electrically paced at 1 Hz by field stimulation. Experiments were performed at 37°C. Intracellular Ca^{2+} transients of isolated cardiomyocytes were measured by fluorescence strength (excitation light: 510 nm; emitted light: 340 nm and 380 nm) loaded with Fura-2/AM for 20 min. Quantitative changes in intracellular Ca^{2+} concentration ($[\text{Ca}^{2+}]_i$) are presented as the ratio of the Fura-2 fluorescence signals (F340/F380) after background fluorescence subtraction.

In situ hybridization in whole-mount zebrafish embryos

In situ hybridization (ISH) was performed in whole-mount zebrafish embryos at two developmental stages of 48 h postfertilization and adulthood, using the following antisense probes: MYL12.1 (ZDB-GENE-030131-4918), MYL12.2 (ZDB-GENE-030131-9028) and CMLC2

(ZDB-GENE-991019-3).⁴⁵ For the preparation of the probes, we amplified and subcloned the cDNA using these primers: GCCACGTCCA ATGTCTTCGC and ggtaatacactactatagggcCCACGAGAGCCCTGAACTTA for MYL12.1; GTTTGCCATGTTTCGACCAGT and ggtaatacactactatagggcTCCCTTTTGCCTACTACCCCAT for MYL12.2; GAACCGGGATGGAGTTATCA and tgtaatacactactatagggcCCTTAAAC CAAATGT for CMLC2.

Generation of the MYL12.1^{-/-} zebrafish

The MYL12.1^{+/-} zebrafish was generated by using the CRISPR/Cas9 technique as previously described.⁴⁶ A gMy12.1 targeting the exon 2 (5'-GATCGACCAGAACCGCGA-3') was designed to make mutations in MYL12.1 gene. DNA was extracted from the tail clipping of adult F1, and genotypes were characterized by PCR-Sanger sequencing. The sequences for PCR primers are: 5'-GTAGGTAAAACCAAATA CAGCCA-3' and 5'-CCAAGGTAATCAACCCGTCAG- 3'.

Characterization of cardiac function in zebrafish

To assess the cardiac function of adult zebrafish we utilized a high-resolution small animal ultrasound imaging system (Vevo 3100LT) to capture echocardiography images of their hearts. The resulting images were subjected to analysis using LV Trace software to quantitatively evaluate cardiac function.

Intramyocardial delivery of AAV9 virus

Mice anesthetized with sodium pentobarbital intraperitoneally were placed in a supine position and orally intubated. Artificial respiration was maintained with a rodent ventilator (R415, RWD Life Science, USA). The heart was exposed upon opening the left pleural cavity by cutting the left third and fourth ribs and intercostal muscles. The pericardium was removed, and a syringe fitted with a 29-G needle was used to inject virus directly into the left ventricle myocardium at three positions. Each mouse was injected with 5×10^{11} vg (virus genomes) in a 20 μ L final volume in saline.

QUANTIFICATION AND STATISTICAL ANALYSIS

Statistical analyses were performed using GraphPad Prism 9.0. All experiments were repeated at least three times and the distribution of data points are presented as means \pm SEM. The unpaired t-test was used for comparison of two conditions, and ANOVAs with *post hoc* multiple-comparisons test were utilized for comparison of three or more conditions. A *p* value less than 0.05 was considered to be statistically significant.